summarized in Table 1, all data for untilted specimens, 15 of 20 for 20 deg, 19 of 45 for 45 deg and only 18 of 62 for 60 deg are of high quality. Others were less good but reasonable, with temperature factors in the direction vertical to their tilt axes in the range between 55 and 180 $Å^{-2}$. As a result, the data quality in the direction normal to the tilt axis was poorer at resolutions beyond 4.0 Å, especially in that taken around the 60 deg tilt angle. These phases improved by solvent flattening using the program DM[22] with the molecular envelope determined from the 5-Å resolution initial map, which was obtained accordingly[5]. The calculated phases were combined with the experimental phases. The figures-of-merit (f.o.m.) calculated from the signal-to-noise ratio of the Fourier components in the image processing[5,6] were close to 1.0 and thus too strongly influenced the combination between observed and calculated phases in DM. After several trials in weighting according to resolutions or to the location in reciprocal space, a simple multiplication of all the f.o.m. by 0.8 produced good weightings schema for the phase combination. Further improvement of the signal-to-noise ratio in the map was achieved by averaging the solvent-flattened density and the density calculated from ideal polyalanine α-helices placed to fit in the density. The Ramachandran plot calculated with PROCHECK from the resulting model contains 81% of the residues in the most favourable region; no residues are in the disallowed region of the plot. A simple preliminary positional refinement (fixed *B*-factors) of the current model by XPLOR produced *R*-factor of 24% and free *R*-factor of 37% starting with initial value of 44%. Only the original F_o map calculated with recombined phases and averaged density and the model at the early stage were presented.

Received 21 October 1996; accepted 2 June 1997

1. Oesterhelt, D. & Stoeckenius, W. Rhodopsin-like protein from the purple membrane of *Halobacterium halobium*. *Nature New Biol.* **233,** 149–152 (1971).
2. Oesterhelt, D. & Stoeckenius, W. Functions of a new photoreceptor membrane. *Proc. Natl Acad. Sci. USA* **70,** 2853–2857 (1973).
3. Khorana, H. G. Bacteriorhodopsin, a membrane protein that uses light to translocate protons. *J. Biol. Chem.* **263,** 7439–7442 (1988).
4. Lanyi, J. K. Proton translocation mechanism and energetics in the light-driven pump bacteriorhodopsin. *Biochim. Biophys. Acta* **1183,** 241–261 (1993).
5. Henderson, R. *et al.* A model for the structure of bacteriorhodopsin based on high resolution electron cryo-microscopy. *J. Mol. Biol.* **213,** 899–929 (1990).
6. Grigorieff, N., Ceska, T. A., Downing, K. H., Baldwin, J. M. & Henderson, R. Electron-crystallographic refinement of the structure of bacteriorhodopsin. *J. Mol. Biol.* **259,** 393–421 (1996).
7. Fujiyoshi, Y. *et al.* Development of a superfluid helium stage for high-resolution electron microscopy. *Ultramicroscopy* **38,** 241–251 (1991).
8. Sakata, K., Tahara, Y., Morikawa, K., Fujiyoshi, Y. & Kimura, Y. A method for observing cross-sectional views of biomembranes. *Ultramicroscopy* **45,** 253–261 (1992).
9. Gerwert, K., Hess, B., Soppa, J. & Oesterhelt, D. The role of 96 Asp in proton translocation by bacteriorhodopsin. *Proc. Natl Acad. Sci. USA* **86,** 4943–4947 (1989).
10. Otto, H. *et al.* Aspartic acid-96 is the internal proton donor in the reprotonation of the Schiff base of bacteriorhodopsin. *Proc. Natl Acad. Sci. USA* **86,** 9228–9232 (1989).
11. Braiman, M. S. *et al.* Vibrational spectroscopy of bacteriorhodopsin mutants: light-driven proton transport involves protonation changes of aspartic acid residues 85, 96, and 212. *Biochemistry* **27,** 8516–8520 (1988).
12. Kimura, Y. & Ikegami, A. Local dielectric properties around polar region of lipid bilayer membranes. *J. Membr. Biol.* **85,** 225–231 (1985).
13. Brown, L. S. *et al.* Glutamic acid 204 is the terminal proton release group at the extracellular surface of bacteriorhodopsin. *J. Biol. Chem.* **270,** 27122–27126 (1995).
14. Kushwaha, S. C., Kates, M. & Stoeckenius, W. Comparison of purple membrane from *Halobacterium cutirubrum* and *Halobacterium halobium*. *Biochim. Biophys. Acta* **426,** 703–710 (1976).
15. Subramaniam, S., Greenhalgh, D. A. & Khorana, H. G. Aspartic acid 85 in bacteriorhodopsin functions both as proton acceptor and negative counterion to the Schiff base. *J. Biol. Chem.* **267,** 25730–25733 (1992).
16. Riesle, J., Oesterhelt, D., Dencher, N. A. & Heberle, J. D38 is an essential part of the proton translocation pathway in bacteriorhodopsin. *Biochemistry* **35,** 6635–6643 (1996).
17. Mogi, T., Stern, L. J., Marti, T., Chao, B. H. & Khorana, H. G. Aspartic acid substitutions affect proton translocation by bacteriorhodopsin. *Proc. Natl Acad. Sci. USA* **85,** 4148–4152 (1988).
18. Oesterhelt, D. & Stoeckenius, W. Isolation of the cell membrane of *Halobacterium halobium* and its fractionation into red and purple membrane. *Methods Enzymol.* **31,** 667–678 (1974).
19. Seiff, F., Wallat, I., Ermann, P. & Heyn, M. A neutron diffraction study on the location of the polyene chain of retinal in bacteriorhodopsin. *Proc. Natl Acad. Sci. USA* **82,** 3227–3231 (1985).
20. Baldwin, J. & Henderson, R. Measurement and evaluation of electron diffraction patterns from two-dimensional crystals. *Ultramicroscopy* **14,** 319–333 (1984).
21. Ceska, T. A. & Henderson, R. Analysis of high-resolution electron diffraction patterns from purple membrane labeled with heavy atoms *J. Mol. Biol.* **213,** 539–560 (1990).
22. Collaborate Computational Project No. 4 *Acta Crystallogr. D* **50,** 760–763 (1994).
23. International Union of Crystallography *International table for Crystallography Volume C: Mathematical, Physical and Chemical Tables* (corrected edn) (ed. Wilson, A. J. C.) (Kluwer, Dordrecht, 1995).

Acknowledgements. We thank M. Ikehara for encouragement and support; W. Kühlbrandt and D. N. Wang for help with data processing; R. Henderson, S. Fuller, J. Lanyi, W. Stoeckenius, Y. Harada and J. Sasaki for helpful discussions; T. Miyata for preparing this manuscript; and Digital Equipment Corporation for help with computers.

Correspondence and requests for materials should be addressed to Y.K. (e-mail: kimuray@beri.co.jp). The coordinates of bacteriorhodopsin reported in this paper have been deposited in the Protein Data Bank (Brookhaven), submission no. PDB BNL-6773; id code awaiting assignment.

erratum

Cofilin promotes rapid actin filament turnover *in vivo*

Pekka Lappalainen & David G. Drubin

Nature **388,** 78–82 (1997)

Figure 3a of this Letter was incomplete as published, with two curves being omitted as a result of an error in the reproduction process. The correct figure is shown here.

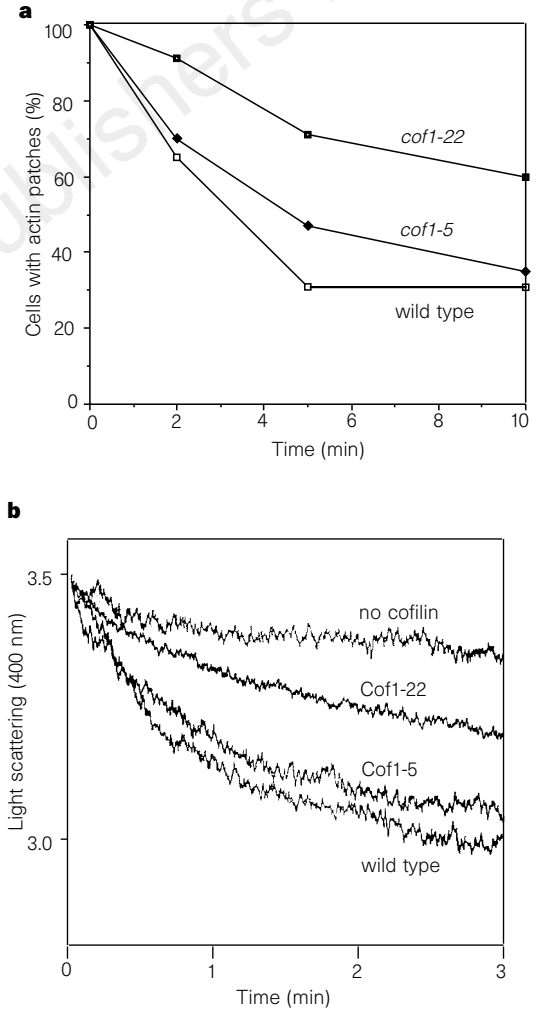

Figure 3 The effects of cofilin mutations on actin-filament depolymerization *in vivo* and *in vitro*. **a**, The percentage of cells with visible actin-filament structures in wild-type, *cof1-5* and *cof1-22* cells at different times after the addition of Lat-A at 25 °C was quantified by rhodamine–phalloidin staining and fluorescent microscopy. For each strain and time point, at least 200 cells from two independent experiments were scored for the presence of actin patches. **b**, The F-actin depolymerization stimulated by recombinant wild-type, *Cof1-5* and *Cof1-22* cofilin was followed by the decrease in light-scattering at 400 nm. Note that dilution of 5 μM yeast actin filaments to 0.5 μM in the absence of cofilin results in slow actin-filament depolymerization. Wild-type cofilin and Cof1-5 cause large increases in the rates of depolymerization, whereas recombinant Cof1-22 causes only a small increase in actin-filament depolymerization rates. The cofilin and yeast actin samples used in these experiments were more than 99% and 95% pure, respectively, based on Coomassie-stained SDS gels (data not shown).

will appear in the DDBJ, EMBL and GenBank databases under the accession number AB002086.

Northern blotting utilized an MTN blot (Clontech) containing poly(A)$^+$ RNA from eight rat tissues (2 μg per lane resolved on a denaturing formaldehyde–agarose gel and transferred to nylon membrane). The full-length cDNA probe was prepared by hexamer-primed labelling (Boehringer Mannheim).

Preparation of His_6-p47. The coding sequence of p47 was amplified without the initiator ATG but with flanking *Bam*HI and *Sal*I sites and cloned into pQE-30 (QIAGEN). The expressed protein was purified using Ni-NTA–agarose (Invitrogen) and high-performance Q (Pharmacia).

Light scattering. Measurements were carried out using a miniDAWN machine, following the manufacturer's instructions.

Electron microscopy. Samples were adsorbed on to carbon-coated Formvar grids and negatively stained with 1% uranyl acetate before air-drying. Grids were viewed using a JEOL 1010 electron microscope at 80 kV with a 70 μm objective aperture. Selected images were aligned and filtered using SEMPER software[24].

Reassembly assay. NEM-treated mitotic Golgi fragments (10–20 μg)[8] were incubated with (final concentrations): rat liver cytosol (30% ammonium sulphate cut; 7.9 mg ml^{-1}); pure p97 (20 μg ml^{-1}; ~220 nM); His_6-p47 (15 μg ml^{-1}; ~320 nM); a mixture of His_6-p47 and p97 (p97: 20 μg ml^{-1}; ~220 nM; His_6-p47: 0 to 60 μg ml^{-1}, 0 to ~1.3 μM), preincubated for 30 min on ice before addition to the assay. After incubation for 60 min at 37 °C, samples were processed for electron microscopy and the percentage of membrane in cisternae estimated[8].

Received 11 March; accepted 30 April 1997.

1. Rothman, J. E. & Warren, G. Implications of the SNARE hypothesis for intracellular membrane topology and dynamics. *Curr. Biol.* **4,** 220–233 (1994).
2. Rothman, J. E. & Wieland, F. T. Protein sorting by transport vesicles. *Science* **272,** 227–234 (1996).
3. Pryer, N. K., Wuestehube, L. J. & Schekman, R. Vesicle-mediated protein sorting. *Annu. Rev. Biochem.* **61,** 471–516 (1992).
4. Ferro-Novick, S. & Jahn, R. Vesicle fusion from yeast to man. *Nature* **370,** 191–193 (1994).
5. Nuoffer, C. & Balch, W. E. GTPases—multifunctional molecular switches regulating vesicular traffic. *Annu. Rev. Biochem.* **63,** 949–990 (1994).
6. Schiavo, G., Rossetto, O. & Montecucco, C. Clostridial neurotoxins as tools to investigate the molecular events of neurotransmitter release. *Sem. Cell Biol.* **5,** 221–229 (1994).
7. Pfeffer, S. R. Transport vesicle docking: SNAREs and associates. *Annu. Rev. Cell Dev. Biol.* **12,** 441–461 (1996).
8. Rabouille, C., Levine, T. P., Peters, J. M. & Warren, G. An NSF-like ATPase, p97, and NSF mediate cisternal regrowth from mitotic Golgi fragment. *Cell* **82,** 905–914 (1995).
9. Acharya, U. *et al.* The formation of Golgi stacks from vesiculated Golgi membranes requires two distinct fusion events. *Cell* **82,** 895–904 (1995).
10. Latterich, M., Frohlich, K. U. & Schekman, R. Membrane fusion and the cell cycle: Cdc48p participates in the fusion of ER membranes. *Cell* **82,** 885–893 (1995).
11. Warren, G. Membrane partitioning during cell division. *Annu. Rev. Biochem.* **62,** 323–348 (1993).
12. Peters, J.-M. *et al.* Ubiquitous soluble Mg^{2+}-ATPase complex: A structural study. *J. Mol. Biol.* **223,** 557–571 (1992).
13. Peters, J. M. & Walsh, M. J. & Franke, W. W. An abundant and ubiquitous homo-oligomeric ring-shaped ATPase particle related to the putative vesicle fusion proteins, Sec18p and NSF. *EMBO J.* **9,** 1757–1767 (1990).
14. Confalonieri, F., Marsault, J. & Duguet, M. SAV, an archaebacterial gene with extensive homology to a family of highly conserved eukaryotic ATPases. *J. Mol. Biol.* **235,** 396–401 (1994).
15. Scherens, B., el Bakkoury, M., Vierendeels, F., Dubois, E. & Messenguy, F. Sequencing and functional analysis of a 32,560 bp segment on the left arm of yeast chromosome II. Identification of 26 open reading frames, including the KIP1 and SEC17 genes. *Yeast* **9,** 1355–1371 (1993).
16. Zhang, S., Guha, S. & Volkert, F. C. The *Saccharomyces SHP1* gene, which encodes a regulator of phosphoprotein phosphatase 1 with differential effects on glycogen metabolism, meiotic differentiation, and mitotic cell cycle progression. *Mol. Cell. Biol.* **15,** 2037–2050 (1995).
17. Tu, J. L., Song, W. J. & Carlson, M. Protein phosphatase type I interacts with proteins required for meiosis and other cellular processes in *Saccharomyces cerevisiae*. *Mol. Cell. Biol.* **16,** 4199–4206 (1996).
18. Sutton, A., Lin, F. & Arndt, K. T. The SIT4 protein phosphatase is required in late G1 for progression into S phase. *Cold Spring Harb. Symp. Quant. Biol.* **56,** 75–81 (1991).
19. Frohlich, K.-U. *et al.* Yeast cell cycle protein CDC48p shows full-length homology to the mammalian protein VCP and is a member of a protein family involved in secretion, peroxisome formation, and gene expression. *J. Cell Biol.* **114,** 443–453 (1991).
20. Rabouille, C., Misteli, T., Watson, R. & Warren, G. Reassembly of Golgi stacks from mitotic Golgi fragments in a cell-free system. *J. Cell Biol.* **129,** 605–618 (1995).
21. Sutton, C. W. *et al.* Identification of myocardial proteins from two-dimensional gels by peptide mass fingerprinting. *Electrophoresis* **16,** 308–316 (1995).
22. Coull, J. M., Pappin, D. J., Mark, J., Aebersold, R. & Koster, H. Functionalized membrane supports for covalent protein microsequence analysis. *Analyt. Biochem.* **194,** 110–120 (1991).
23. Hunt, D. F., Yates, J. R., Shabanowitz, J., Winston, S. & Hauer, C. R. Protein sequencing by tandem mass spectrometry. *Proc. Natl Acad. Sci. USA* **83,** 6233–6237 (1986).
24. Saxton, W. O. Semper: distortion compensation, selective averaging, 3-D reconstruction, and transfer function correction in a highly programmable system. *J. Struct. Biol.* **116,** 230–236 (1996).

Acknowledgements. We thank T. Chappell, F. Barr, B. Svejstrup, B. Sönnichsen, M. Lowe, C. Fernandez, D. Shima, J. Shorter, N. Hui and A. Coffer for helpful comments and for reagents; G. Banting for the rat liver cDNA library; J.-M. Peters for monoclonal anti-p97 antibodies; G. Clark and A. Davies for DNA sequencing; and D. Rahman for protein sequencing. Special thanks go to N. Nakamura for advice.

Correspondence and requests for materials should be addressed to G.W. (e-mail: g.warren@europa.lif.icnet.uk).

Cofilin promotes rapid actin filament turnover *in vivo*

Pekka Lappalainen & David G. Drubin

Department of Molecular and Cell Biology, 401 Barker Hall, University of California, Berkeley, California 94720, USA

The ability of actin filaments to function in cell morphogenesis and motility is coupled to their capacity for rapid assembly and disassembly. Because disassembly *in vitro* is much slower than *in vivo*, cellular factors that stimulate disassembly have long been assumed to exist. Although numerous proteins can affect actin dynamics *in vitro*, demonstration of *in vivo* relevance of these effects has not been achieved. We have used genetics and an actin-inhibitor in yeast to demonstrate that rapid cycles of actin assembly and disassembly depend on the small actin-binding protein cofilin, and that cofilin stimulates filament disassembly. These results may explain why cofilin is ubiquitous in eukaryotes and is essential for viability in every organism in which its function has been tested genetically. Magnitudes of disassembly defects in cofilin mutants *in vivo* were found to be correlated closely with the magnitudes of disassembly defects observed *in vitro*, supporting our conclusions. Furthermore, these cofilin

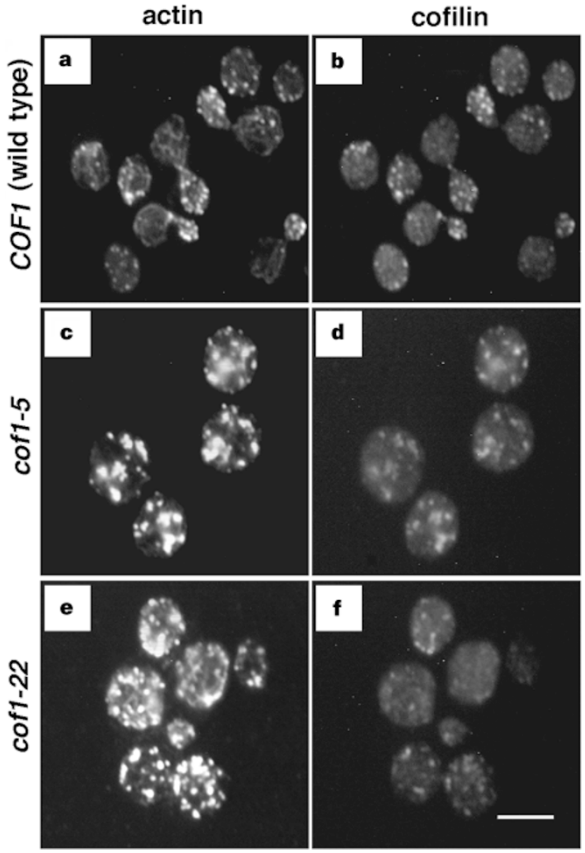

Figure 1 Cells were grown at 20 °C to A_{600} = 0.3, shifted to 34 °C for 3 h and fixed with 5% formaldehyde. The actin and cofilin in wild-type (**a**, **b**), *cof1-5* (**c**, **d**) and *cof1-22* (**e**, **f**) were visualized by immunofluorescence. In the wild-type cells, the actin patches are well polarized and actin cables are visible in the cells that are displaying polarized growth. Cofilin localizes to cortical actin patches. In *cof1-5* and *cof1-22* cells shifted to 34 °C the actin patches are very large, irregularly shaped and almost completely depolarized. In both mutants, cofilin localizes mostly to these actin structures. Scale bar, 5 μm.

mutants provided an opportunity to distinguish in living cells those actin functions that depend specifically on filament turnover (endocytosis) from those that do not (cortical actin patch motility).

Cofilin is a member of the cofilin/ADF family of small (M_r 15K–20K) actin-binding proteins[1]. These proteins bind to actin monomers (G-actin) and actin filaments (F-actin) *in vitro*, and stimulate depolymerization of actin filaments in a pH-dependent manner[2–5]. Despite a wealth of biochemical data, little is known about the function of cofilin and related proteins *in vivo*. Every eukaryotic cell type examined contains at least one member of this family, suggesting that cofilin performs a universally important function[1]. This conclusion is further supported by the observations that in *Saccharomyces cerevisiae*, *Drosophila melanogaster* and *Caenorhabditis elegans*, null mutations in the cofilin/ADF genes are lethal[6–8]. However, the lack of partial loss-of-function mutations in cofilin had previously precluded tests of the roles of this protein in living cells.

We have studied the contribution of cofilin to actin cytoskeleton dynamics in yeast by using two temperature-sensitive cofilin alleles that were isolated in a systematic mutational analysis of the *S. cerevisiae COF1* gene (P.L. *et al.*, unpublished results). In both alleles, a cluster of charged residues (Asp 10 and Glu 11 in *cof1–5*, and Glu 134, Arg 135 and Arg 138 in *cof1–22*) are replaced by alanines. The mutant alleles were integrated into the yeast genome and their phenotypes examined in haploid segregants. At temperatures suitable for robust growth (20–25 °C), *cof1–5* and *cof1–22* strains show similar growth rates and morphology to wild-type cells. The actin 'patches', which are F-actin structures associated with the cell cortex[9], are slightly brighter in *cof1–5* and *cof1–22* cells than in wild-type cells, but overall organization of the cytoskeleton seems to be normal, and actin levels in these mutants are unchanged within the sensitivity of quantitative western blots (±20%). At a temperature that was non-permissive for growth (34 °C), *cof1–5* and *cof1–22* cells became enlarged and their cortical actin patches lost their characteristic asymmetric localization (Fig. 1). After incubation at 34 °C for 3 h, 15–20% of the mutant cells have multiple nuclei. The actin patches in both *cof1–5* and *cof1–22* cells are unusually large (Fig. 1), consistent with the possibility that these cells have severe defects in actin filament turnover.

To examine the effects of these mutations on F-actin turnover rates *in vivo*, we used latrunculin-A (Lat-A), an actin monomer-sequestering drug. Lat-A binds close to the nucleotide-binding pocket of actin monomers, and prevents actin filament assembly while allowing disassembly[10,11]. In living yeast cells, Lat-A causes a rapid and specific disruption of the actin cytoskeleton[11]. Because Lat-A functions by sequestering actin monomers, the rate of disappearance of actin structures is expected to reflect the rate of subunit dissociation from actin filaments *in vivo*[11]. The Lat-A actin-filament disassembly assay was performed at both 25 °C and 34 °C. The rates of disassembly in wild-type and cofilin mutant strains seem to be independent of temperature. The data from the depolymerization assay at 25 °C are presented in Figs 2 and 3a. In wild-type cells, most of the actin patches disappear within 2 min of addition of a high concentration (400 μM) of Lat-A. After 5 min only ~30% of the wild-type cells have any visible actin-filament structures when visualized by rhodamine–phalloidin staining (Figs 2 and 3a). The proportion of cells with faint actin-filament staining remains unchanged at 10 min. The rate of disappearance of actin patches in *cof1–5* cells is slightly reduced compared with wild-type cells, whereas the patches in *cof1–22* cells disappear much more slowly (Figs 2 and 3a). Most of the *cof1–22* cells still had many bright actin patches 10 min after the addition of Lat-A, indicating that this cofilin mutation causes a dramatic decrease in the F-actin depolymerization rate *in vivo* (the intensity and number of actin patches in Fig. 2i (*cof1–22*, 10 min) is greater than in Fig. 2b (*COF1*, 2 min)). The total disappearance of actin filament structures in *cof1–22* cells takes approximately 20 min (data not shown).

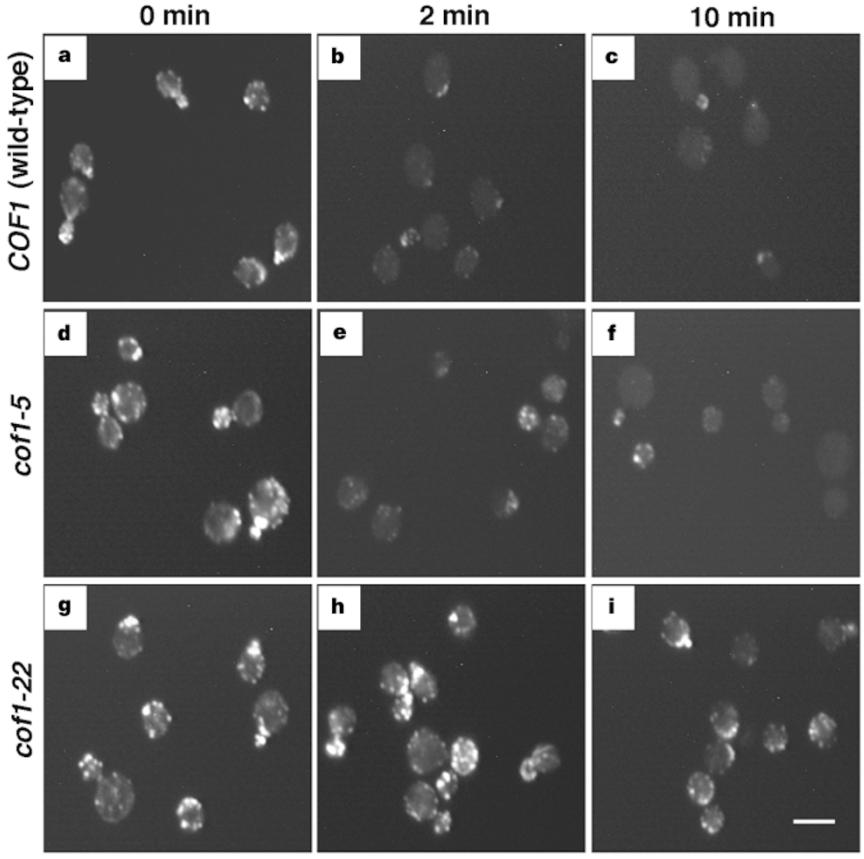

Figure 2 Filamentous actin was visualized by rhodamine-phalloidin staining in wild-type (**a**–**c**), *cof1-5* (**d**–**f**) and *cof1-22* (**g**–**i**) strains at 0, 2 and 10 min after the addition of 400 μM Lat-A to the cultures at 25 °C. In wild-type and *cof1-5* cells, the actin filaments disappear rapidly. After 2 min cells have either very faint actin patches or none at all. In contrast, actin patches in *cof1-22* cells disappear >5-fold more slowly than in the wild type. Even after 10 min, most of the *cof1-22* cells have brightly stained actin patches. All photographs were taken using identical microscope and imaging-system settings. Scale bar, 5 μm.

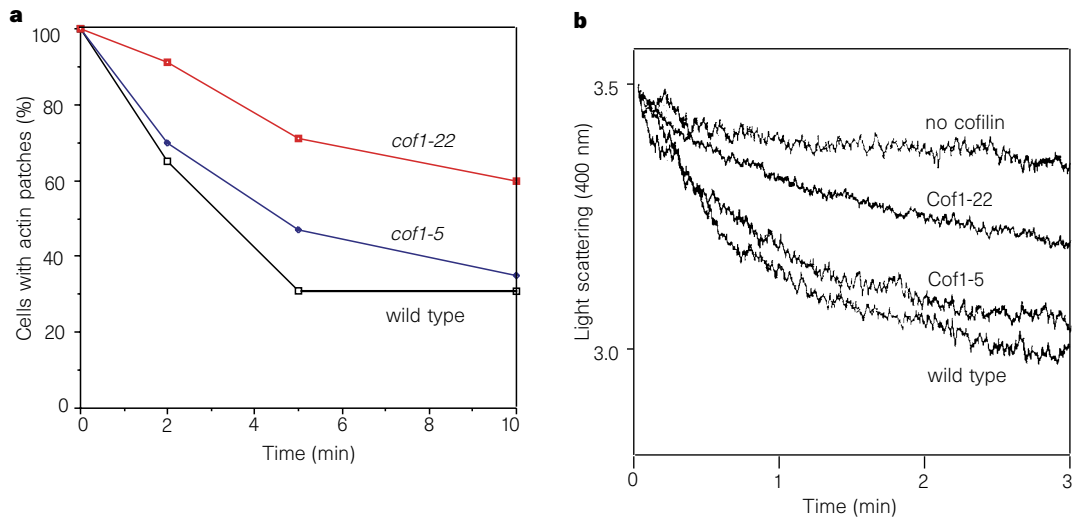

Figure 3 The effects of cofilin mutations on actin-filament depolymerization *in vivo* and *in vitro*. **a**, The percentage of cells with visible actin-filament structures in wild-type, *cof1–5* and *cof1–22* cells at different times after the addition of Lat-A at 25 °C was quantified by rhodamine–phalloidin staining and fluorescent microscopy. For each strain and time point, at least 200 cells from two independent experiments were scored for the presence of actin patches. **b**, The F-actin depolymerization stimulated by recombinant wild-type, *Cof1–5* and *Cof1–22* cofilin was followed by the decrease in light-scattering at 400 nm. Note that dilution of 5 μM yeast actin filaments to 0.5 μM in the absence of cofilin results in slow actin-filament depolymerization. Wild-type cofilin and Cof1–5 cause large increases in the rates of depolymerization, whereas recombinant Cof1–22 causes only a small increase in actin-filament depolymerization rates. The cofilin and yeast actin samples used in these experiments were more than 99% and 95% pure, respectively, based on Coomassie-stained SDS gels (data not shown).

The relative rates of F-actin depolymerization measured *in vivo* for the cofilin mutants correlate well with the rates by which they promote F-actin depolymerization *in vitro*. Recombinant Cof1–5 and Cof1–22 mutants were expressed and purified. In fluorescence-monitored urea denaturation assays, both mutants show simple two-state unfolding transitions, indicating that the preparations consist of homogeneous populations of protein (P.L. *et al.*, unpublished results). To assay depolymerization rates *in vitro*, actin filaments were first assembled from purified yeast actin. They were then diluted 10-fold with or without recombinant wild-type, Cof1–5 or Cof1–22 yeast cofilin. The depolymerization of actin filaments was followed by a decrease in light scattering at 400 nm. In this *in vitro* assay, performed at 25 °C and 37 °C, Cof1–5 showed a small defect in actin-filament depolymerization, and Cof1–22 showed a pronounced defect in actin-filament depolymerization relative to wild-type cofilin (Fig. 3b). The magnitudes of these defects were not affected by temperature. Because Cof1–5 showed only a very small depolymerization defect in our *in vivo* and *in vitro* assays, it is possible that the temperature sensitivity of this mutant results from some currently unidentified activity of cofilin, or that the small decrease in actin dynamics precludes cell growth at elevated temperatures. When the *in vitro* depolymerization assay was performed by adding 100 μM Lat-A and 1 μM cofilin to 5 μM actin filaments, results similar to those in Fig. 3b were obtained, indicating that Lat-A does not affect the rate of cofilin-stimulated actin depolymerization (data not shown).

To test the specificity of the effects for cofilin, we applied the Lat-A assay to yeast strains carrying deletions in genes that encode other proteins important for actin cytoskeleton organization (*SLA2*, *SAC6* and *SRV2*)[12–14]. In these strains, disappearance of actin patches follows kinetics similar to those observed for their wild-type parent strains (data not shown). As *sac6* and *sla2* mutants are defective in endocytosis, these results demonstrate that endocytosis defects do not impair the entry of Lat-A into yeast cells. Further, *cof1–5* and *cof1–22* strains showed fivefold and fourfold greater sensitivity to Lat-A, respectively, than the wild type, further suggesting that these strains do not have defects in Lat-A uptake (data not shown).

The availability of cofilin mutants that cause a dramatic decrease in actin-filament turnover provided an opportunity to determine the role of actin-filament turnover in living cells. Many components in the yeast cortical actin cytoskeleton have been shown to be important for endocytosis[13,15,16]. To test specifically whether the F-actin turnover induced by cofilin is necessary for endocytosis, we followed the uptake of a fluid-phase marker, lucifer yellow, in *cof1–5* and *cof1–22* strains. At temperatures permissive for robust cell growth (20 and 25 °C), *cof1–5* and *cof1–22* cells show severe defects in the uptake of lucifer yellow (Fig. 4a), indicating that rapid turnover of cortical actin structures is essential for endocytosis. Consistent with this possibility, the cofilin mutant with the most dramatic effects on actin turnover, *cof1–22*, had the most dramatic effects on endocytosis. It is possible that the temperature-sensitive phenotype of *cof1–5* and *cof1–22* mutants results from the defect in endocytosis, as an apparent dependence on endocytosis for growth at high temperatures has been reported[17]. Alternatively, cells may have a higher requirement for F-actin depolymerization at higher temperatures, or there could be another cofilin-dependent reaction that is sensitive to temperature.

Yeast cortical actin patches have recently been shown to translocate within the plane of the cell cortex with a velocity up to 1.5 $\mu m\,s^{-1}$ (refs 18, 19). As these studies failed to demonstrate a role for any known myosins in this motility[18], it has been suggested that the actin-patch movement might be driven by a filament turnover mechanism similar to that which drives intracellular movement of *Listeria monocytogenes*[20]. To test whether actin-filament turnover is required for this motility, we transformed wild-type and *cof1–22* mutant strains with a plasmid expressing a green fluorescent protein (GFP)–Abp1 fusion protein that localizes specifically to cortical actin structures[19]. At permissive temperature (20–25 °C) the cortical actin patches give strong fluorescence and show rapid movements (Fig. 4b). The quantified data from approximately 700 actin-patch movements in wild-type and *cof1–22* mutant cells is shown in Fig. 4c. There are no significant differences either in the speed distribution or in the observed maximum velocity of actin patches between wild type and the *cof1–22* mutant strain. Because the *cof1–22* mutant shows a large decrease in actin-filament turnover *in vivo*, these results suggest that

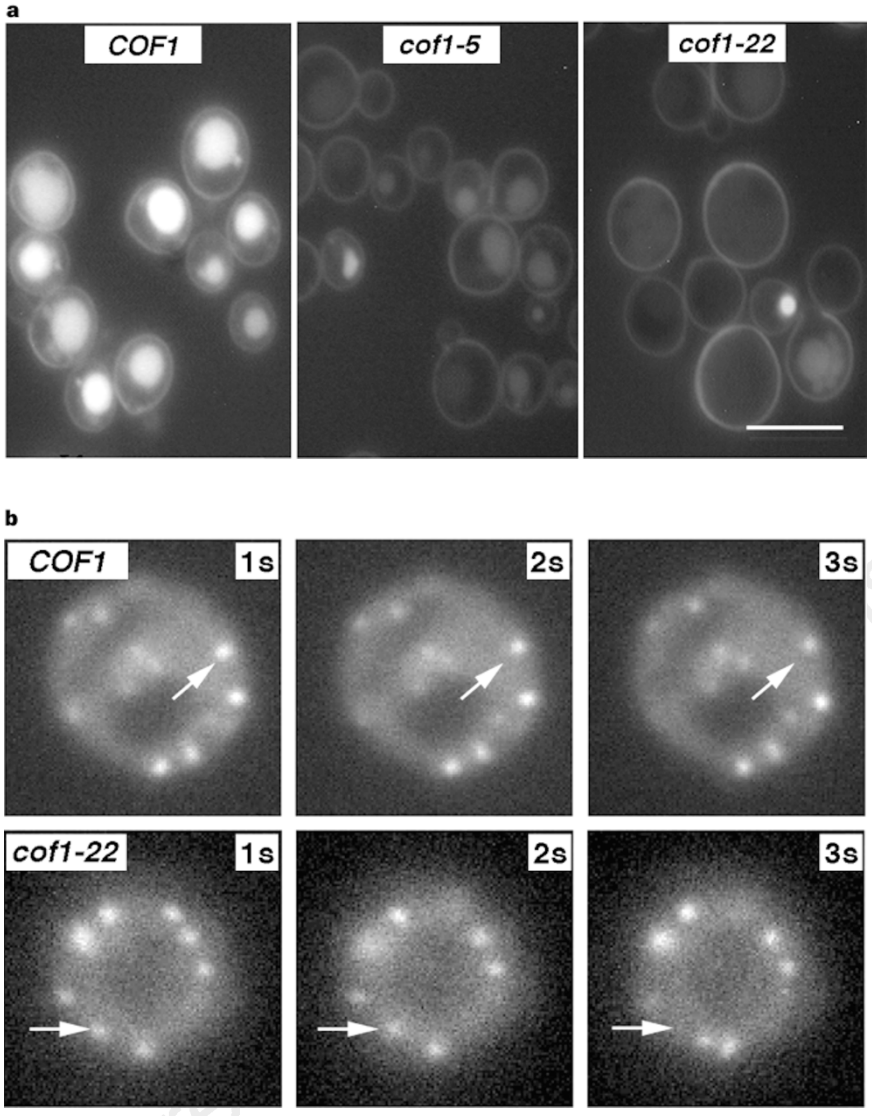

Figure 4 Effects of cofilin mutants on endocytosis and actin patch movement. **a**, The uptake of lucifer yellow in wild-type, *cof1–5* and *cof1–22* cells after 2 h of incubation at 25 °C was visualized by fluorescence microscopy. Vacuoles in wild-type cells show bright staining, whereas in *cof1–5* and *cof1–22* cells the uptake of lucifer yellow into vacuoles is defective. Scale bar, 5 μm. **b**, Representative data from the actin-patch movement in *COF1* (wild type) and *cof1–22* strains. The interval between each frame is 1 s. The reference arrows mark the same position in each frame. The size of each frame is 6.6 μm × 6.6 μm. **c**, Histogram of speeds of actin patches in *COF1* (wild type) and *cof1–22* strains. The speed is calculated from the distance that the patches have moved in the *x*–*y* plane between two frames.

actin-patch motility is not driven by filament turnover. In support of this conclusion, we find that patch motility is unaffected by sequestration of free actin monomers through the addition of high concentrations of Lat-A to cells (P.L. and L. Belmont, unpublished data). Patches continued to move even as they were disassembling.

In conclusion, we have provided evidence that members of the cofilin/ADF family promote actin-filament depolymerization *in vivo* and are required for rapid cycles of actin assembly and disassembly. It has been shown that cofilin/ADF promotes actin-filament depolymerization in cell extracts[21,22]. Our data extend this observation to living cells, and identify a process in which rapid turnover of actin filaments is essential. These findings, considered with the intimate coupling of actin dynamics with actin function, may explain why cofilin is expressed ubiquitously and is essential for viability in every cell type in which its gene has been mutated. The actin-associated activities of cofilin have been shown to be regulated by pH, phosphorylation and phosphoinositides[3,23–25]. However, as we were unable to detect any differences in Lat-A-induced disassembly rates among cells at different stages of the cell cycle (data not shown), our data indicate that in yeast, cofilin is active throughout the cell cycle. Despite speculation that cortical actin-patch motility might be driven by an assembly coupled mechanism akin to that in *Listeria* bacteria[20], loss of cofilin function did not have consequences for cortical actin-patch motility. Considered with a previous study that failed to find an effect of mutation of any of the yeast myosin genes on patch motility[18], our findings suggest that patch motility might be driven by a different mechanism. □

Methods

Yeast strains. The construction of *cof1* mutants will be described in more detail elsewhere (P.L. *et al.*, unpublished data). Briefly, the *LEU2* marker was inserted 91 base pairs downstream from the end of the cofilin open reading frame (ORF) in pBluescript SK plasmid (Strategene) carrying *COF1*. The site-directed mutations were created by oligonucleotide-based mutagenesis (Transformer, Clontech). The plasmids were linearized and *COF1*, *cof1–5* and *cof1–22* were integrated into a *COF1/cof1-Δ1::HIS3* hemizygote strain (DDY427). Integrants were identified by screening for loss of the *HIS3* marker and gain of the *LEU2* marker. These cells were sporulated and the phenotypes were scored in haploid segregants. Each mutation was confirmed by PCR amplification and restriction endonuclease digestions. The haploid yeast strains carrying deletions of *SLA2*, *SAC6* and *SRV2* and their parent strains have been described[12,26,27].

Cell biological methods. Yeast cultures were grown in YPD medium at 20 °C, unless stated otherwise. Immunofluorescence was performed as described[6]. The fluid-phase endocytosis assay was performed at 25 °C as described[28]. For the *in vivo* Lat-A depolymerization assay, cells were grown at 20 °C at $A_{600} = 0.2$, and Lat-A was added to cultures to a final concentration of 400 μM. The cells were incubated at 25 or 34 °C and 250-μl samples of cells were fixed at 0, 2 and 10 min with 5% formaldehyde, and actin-filament structures were visualized by rhodamine-phalloidin staining. After staining for

30 min, the cells were washed 5 times with 200 μl PBS + 0.1% TritonX-100, resuspended in 6 μl mounting media and placed on a slide. The sensitivities of wild-type, *cof1–5* and *cof1–22* cells to lat-A were examined in a halo-assay[11] in which filters spotted with Lat-A were deposited on lawns of yeast and the diameter of zones of growth inhibition measured. For actin-patch movement studies, the *COF1* and *cof1–22* strains were transformed with a plasmid carrying GFP linked to Abp1 (ref. 19). Cells from such transformants were grown at 20 °C to an A_{600} of ~0.4, and movement of actin patches was followed with Zeiss Axiovert 100TV microscope. Images from about 400 patches in 5 unbudded cells from each strain were collected using a Princeton Instruments ST-138 camera/controller with a Kodak KAF1400 chip (each pixel is 0.069 μm × 0.069 μm). Frames from the cells were recorded at intervals of 0.95 to 1.25 s and the data analysed using the Animate program (written by A. Mallavarapu). The maximum speeds observed in our study (0.75 μm s^{-1}) are approximately twofold slower than the maximum speeds previously reported[18]. This might result from differences in yeast strain backgrounds or the differences in the time resolution of image acquisition (the camera system in ref. 18 recorded frames with 0.2-s intervals compared to ~1-s intervals in this study).

***In vitro* depolymerization assay.** The *COF1* yeast cofilin gene was amplified by PCR, subcloned into pGEX2T vector (Pharmacia), and expressed in *Escherichia coli* JM109 cells as a glutathione *S*-transferase (GST) fusion protein. Site-directed mutations were introduced to pGEX2T-*COF1* plasmid by oligonucleotide-based mutagenesis (Transformer, Clontech). Fusion proteins were purified by glutathione–agarose affinity chromatography[29]. All constructs made by PCR were sequenced to exclude the possibility of undesired mutations. Cofilin was cleaved from GST by thrombin and purified by gel-filtration (Superdex-75, Pharmacia). Yeast actin was purified as described[30] and polymerized in F-buffer comprising (in mM) 20 Tris, pH 7.5, 100 KCl, 2 $MgCl_2$, 0.7 ATP, 0.2 DTT, 0.2 $CaCl_2$, at a final concentration of 5 μM. For the depolymerization assay, F-actin and cofilin were mixed in a cuvette to final concentrations of 0.5 μM, and the depolymerization of F-actin was followed by decrease in light scattering at 400 nm.

Received 13 March; accepted 21 April 1997.

1. Moon, A. & Drubin, D. G. The ADF-cofilin proteins: Stimulus responsive modulators of actin dynamics. *Mol. Biol. Cell* **6,** 1423–1431 (1995).
2. Bamburg, J. R., Harris, H. E. & Weeds, A. G. Partial purification and characterization of an actin depolymerizing factor from brain. *FEBS Lett.* **121,** 178–182 (1990).
3. Yonezawa, N., Nishida, E. & Sakai, H. pH control of actin polymerization by cofilin. *J. Biol. Chem.* **260,** 14410–14412 (1985).
4. Hawkins, M., Pope, B., Maciver, S. K. & Weeds, A. G. Human actin depolymerizing factor mediates a pH-sensitive destruction of actin filaments. *Biochemistry* **32,** 9985–9993 (1993).
5. Hayden, S. M., Miller, P. S., Brauweiler, A. & Bamburg, J. R. Analysis of the interactions of actin depolymerizing factor with G- and F-actin. *Biochemistry* **32,** 9994–10004 (1993).
6. Moon, A. L., Janmey, P. A., Louie, K. A. & Drubin, D. G. Cofilin is an essential component of the yeast cortical cytoskeleton. *J. Cell Biol.* **120,** 421–435 (1993).
7. Gunsalus, K. C. *et al.* Mutations in *twinstar*, a *Drosophila* gene encoding a cofilin-ADF homologue, result in defects in centrosome migration and cytokinesis. *J. Cell Biol.* **131,** 1243–1259 (1995).
8. McKim, K. S., Matheson, C., Marra, M. A., Wakarchuk, M. F. & Baillie, D. L. The *Caenorhabditis elegans unc-60* gene encodes protein homologous to a family of actin binding proteins. *Mol. Gen. Genet.* **242,** 346–357 (1994).
9. Mulholland, J. *et al.* Ultrastructure of the yeast actin cytoskeleton and its association with the plasma membrane. *J. Cell Biol.* **125,** 381–391 (1994).
10. Coue, M., Brenner, S. L., Spector, I. & Korn, E. D. Inhibition of actin polymerization by Latranculin-A. *FEBS Lett.* **213,** 316–318 (1987).
11. Ayscough, K. R. *et al.* High rates of actin filament turnover in budding yeast and roles for actin in establishment and maintenance of cell polarity revealed using the actin inhibitor Latranculin-A. *J. Cell Biol.* **137,** 399–416 (1997).
12. Holtzman, D. A., Yang, S. & Drubin, D. G. Synthetic-lethal interactions identify two novel genes, *SLA1* and *SLA2*, that control membrane cytoskeleton assembly in *Saccharomyces cerevisiae*. *J. Cell Biol.* **122,** 635–644 (1993).
13. Kubler, E. & Riezman, H. Actin and fimbrin are required for the internalization step of endocytosis in yeast. *EMBO J.* **12,** 2855–2862 (1993).
14. Freeman, N. L., Chen, Z., Horenstein, J., Weber, A. & Field, J. An actin monomer binding activity localizes to the carboxyl half of the *Saccharomyces cerevisiae* cyclase associated protein. *J. Biol. Chem.* **270,** 5680–5685 (1995).
15. Geli, M. I. & Riezman, H. Role of type I myosins in receptor-mediated endocytosis in yeast. *Science* **272,** 533–535 (1996).
16. Goodson, H. V. *et al.* Synthetic lethality screen identifies a novel yeast myosin I gene (*MYO5*)—Myosin I proteins are required for polarization of the actin cytoskeleton. *J. Cell Biol.* **133,** 1277–1291 (1996).
17. Benedetti, H., Raths, S., Crauzas, F. & Riezman, H. The *END3* gene encodes a protein that is required for the internalization step of endocytosis and for actin ctyoskeleton organization in yeast. *Mol. Biol. Cell* **5,** 1023–1037 (1994).
18. Waddle, J. A., Karpova, T. S., Waterston, R. H. & Cooper, J. A. Movement of cortical actin patches in yeast. *J. Cell Biol.* **132,** 861–870 (1996).
19. Doyle, T. & Botstein, D. Movement of yeast cortical actin cytoskeleton visualized *in vivo*. *Proc. Natl Acad. Sci. USA* **93,** 3886–3891 (1996).
20. Welch, M. D., Mallavarapu, A., Rosenblatt, J. & Mitchison, T. J. Actin dynamics *in vivo*. *Opin. Cell Biol.* **9,** 54–61 (1997).
21. Rosenblatt, J., Agnew, B. J., Abe, H., Bamburg, J. R. & Mitchison, T. J. *Xenopus* actin depolymerizing factor/cofilin XAC is responsible for the turnover of actin filaments in *Listeria monocytogenes* tails. *J. Cell Biol.* **136,** 1323–1332 (1997).
22. Carlier, M. *et al.* Actin depolymerizing factor (ADF/cofilin) uses ATP hydrolysis to enhance actin dynamics. *J. Cell Biol.* **136,** 1307–1322 (1997).
23. Yonezawa, N., Nishida, E., Iida, K., Yahara, I. & Sakai, H. Inhibition of the interactions of cofilin, destrin and deoxyribonuclease-I with actin by phosphoinositides. *J. Biol. Chem.* **265,** 8382–8386 (1990).
24. Agnew, B. J., Minamide, L. S. & Bamburg, J. R. Reactivation of phosphorylated actin depolymerizing factor and identification of the regulatory site. *J. Biol. Chem.* **270,** 17582–17585 (1995).
25. Abe, H., Obinata, T., Minamide, L. S. & Bamburg, J. R. *Xenopus laevis* actin-depolymerizing factor/cofilin: A phosphorylation-regulated protein essential for development. *J. Cell Biol.* **132,** 871–885 (1996).
26. Adams, A. E. M., Botstein, D. & Drubin, D. G. Requirement of yeast fimbrin for actin organization and morphogenesis *in vivo*. *Nature* **354,** 404–408 (1991).
27. Lila, T. & Drubin, D. G. Evidence for physical and functional interactions among two *Saccharyomyces cerevisiae* SH3 domain proteins, an adenylyl cyclase-associated protein and the actin cytoskeleton. *Mol. Biol. Cell* **8,** 367–385 (1997).
28. Dulic, V. *et al.* Yeast endocytosis assays. *Methods Enzymol.* **194,** 697–710 (1991).
29. Ausubel, F. M. *et al. Current Protocols in Molecular Biology* (John Wiley, New York, 1990).
30. Buzan, J. M. & Frieden, C. Yeast actin: Polymerization kinetic studies of wild-type and a poorly polymerizing mutant. *Proc. Natl Acad. Sci. USA* **93,** 91–95 (1996).

Acknowledgements. We thank K. Ayscough for the Lat-A disassembly procedure; L. Belmont, B. Goode and K. Kozminski for comments on the manuscript; and A. Mallavarapu and T. Mitchison for help in recording patch movements. This work was supported by long-term fellowships from the European Molecular Biology Organization and Human Frontier Science Program (to P.L.) and by grants from the NIH and American Cancer Society (to D.G.D.).

Correspondence and requests for materials should be addressed to D.G.D. (e-mail: drubin@mendel.berkeley.edu).

Mutations increasing autoinhibition inactivate tumour suppressors Smad2 and Smad4

Akiko Hata*, Roger S. Lo*, David Wotton*, Giorgio Lagna† & Joan Massagué*

** Cell Biology Program and Howard Hughes Medical Institute, Memorial Sloan-Kettering Cancer Center, † Laboratory of Molecular Embryology, The Rockefeller University, New York, New York 10021, USA*

Smad2 and Smad4 are related tumour-suppressor proteins[1,2], which, when stimulated by the growth factor TGF-β, form a complex to inhibit growth[3]. The effector function of Smad2 and Smad4 is located in the conserved carboxy-terminal domain (C domain) of these proteins and is inhibited by the presence of their amino-terminal domains (N domain)[4,5]. This inhibitory function of the N domain is shown here to involve an interaction with the C domain that prevents the association of Smad2 with Smad4. This inhibitory function is increased in tumour-derived forms of Smad2 and 4 that carry a missense mutation in a conserved N domain arginine residue. The mutant N domains have an increased affinity for their respective C domains, inhibit the Smad2–Smad4 interaction, and prevent TGFβ-induced Smad2–Smad4 association and signalling. Whereas mutations in the C domain disrupt the effector function of the Smad proteins, N-domain arginine mutations inhibit SMAD signalling through a gain of autoinhibitory function. Gain of autoinhibitory function is a new mechanism for inactivating tumour suppressors.

SMAD proteins are central to signalling by the TGF-β family of growth factors[6]. An effector function of the C domain and an inhibitory function of the N domain of Smad proteins were discovered during studies on the mesoderm-inducing activity of Smad2 in *Xenopus* embryo explants[5] and on the transcriptional activity of various Smad proteins in mammalian cells[4]. SMAD proteins exist as homo-oligomers that form functional hetero-oligomeric complexes in response to TGF-β and related factors[3]. These complexes are formed by association of a pathway-restricted SMAD with the shared SMAD, Smad4 (also known as DPC4 or *deleted in pancreatic carcinoma 4*). Thus Smad1 associates with Smad4 in response to stimulation by bone morphogenic protein